A New Algorithm for Surface Deformation Monitoring Based on Small Baseline Differential SAR Interferograms

Paolo Berardino, *Member, IEEE*, Gianfranco Fornaro, Riccardo Lanari, *Senior Member, IEEE*, and Eugenio Sansosti, *Senior Member, IEEE*

***Abstract*—We present a new differential synthetic aperture radar (SAR) interferometry algorithm for monitoring the temporal evolution of surface deformations. The presented technique is based on an appropriate combination of differential interferograms produced by data pairs characterized by a small orbital separation (baseline) in order to limit the spatial decorrelation phenomena. The application of the singular value decomposition method allows us to easily "link" independent SAR acquisition datasets, separated by large baselines, thus increasing the observation temporal sampling rate. The availability of both spatial and temporal information in the processed data is used to identify and filter out atmospheric phase artifacts. We present results obtained on the data acquired from 1992 to 2000 by the European Remote Sensing satellites and relative to the Campi Flegrei caldera and to the city of Naples, Italy that demonstrate the capability of the proposed approach to follow the dynamics of the detected deformations.**

***Index Terms*—Ground deformations, SAR interferometry, synthetic aperture radar (SAR).**

I. Introduction

DIFFERENTIAL synthetic aperture radar interferometry (DIFSAR) is a relatively new technique that has been successfully used for generating large-scale surface deformation maps on a dense grid (the displacement field being measured in the radar line of sight) and with a centimeter-to-millimeter accuracy [1]. While the DIFSAR approach has been applied several times to the analysis of a single deformation episode [2]–[7], the interest of the scientific community is now progressively moving toward the study of the temporal evolution of the detected deformations, and some results have already been presented in the literature [8]–[13].

An effective way to study the temporal behavior of the detected phenomena is the generation of time-series that allows us to follow the evolution of the monitored deformations; to do this, the information available from each data pair must be properly related to those included in the other acquisitions via the generation of an appropriate sequence of DIFSAR interferograms. A key limitation, in this case, is that data pairs used to generate differential interferograms must be acquired from relatively close tracks (the spatial separation between orbits is referred to as *baseline*) in order to reduce both spatial decorrelation and topography errors. In practical cases, as for the European Remote Sensing (ERS) satellites ERS-1 and ERS-2 sensors, the available acquisitions are generally distributed in small baseline (SB) subsets, separated by large "baselines"; accordingly, only one deformation time series for each subset can be easily obtained [11], [12]. Since these results are typically poorly sampled in time and not directly linkable to those computed from other subsets, the limitation to exploit all the available acquisitions for the generation of an overall deformation time-series is evident.

Some advances in this field have been recently introduced at the expense of the processed area coverage. First of all, it has been demonstrated that small man-made features remain very correlated over time [14], [15], although interferograms over these areas only show pointwise information. Moreover, a new solution for maximizing the number of acquisitions used has been proposed, and the technique is referred to as permanent scatterers (PS) [16], [17]. This approach implies the generation, with respect to a common (master) image, of a DIFSAR interferogram for each available acquisition even if the exploited data pair is characterized by a large baseline (even larger than the critical baseline [1]) and, therefore, affected by baseline decorrelation phenomena. It is evident that, in this case, the use of all the available data acquisitions is accomplished, but at the expense of imaged pixel density; indeed, only those targets that exhibit sufficiently high coherence values, even at large spatial baselines (i.e., the PS targets), are considered, and their density may be in some cases rather low; this often happens, for instance, in nonurban areas.

This work proposes a new DIFSAR approach for the evaluation of the earth's surface deformation *evolution*; it extends the technique presented in [11] and [12] to the case of multiple SB acquisition subsets via an easy and effective combination of all the available SB interferograms. The combination is based on a minimum-norm criterion of the velocity deformation, easily obtained in our case via the application of the singular value decomposition (SVD) method. The presented technique satisfies two key requirements: to increase the "temporal sampling rate" by using all the acquisitions included in the different SB subsets and to preserve the capabilities of the system to provide spatially dense deformation maps, the latter being a key issue of conventional DIFSAR interferometry. Clearly, this latter requirement is

Manuscript received December 27, 2001, revised July 12, 2002. This work was supported in part by the Italian Space Agency, by the European Space Agency, and by the (Italian) National Group for Volcanology (GNV).

The authors are with Istituto per il Rilevamento Elettromagnetico dell'Ambiente, National Research Council of Italy, 80124 Napoli, Italy (e-mail: berardino.p@irea.cnr.it; fornaro.g@irea.cnr.it; lanari.r@irea.cnr.it; sansosti.e@irea.cnr.it).

Digital Object Identifier 10.1109/TGRS.2002.803792

related to the use of small baseline interferograms that limit the baseline decorrelation phenomena. We further remark that our approach is easily implemented as a postprocessing step applied to the set of DIFSAR interferograms that may be generated via already available interferometric data processing tools.

The proposed combination technique relies on the use of unwrapped DIFSAR interferograms, with the unwrapping operation implemented via a two-step processing procedure extending the sparse-grid approach presented in [18]. Moreover, in spite of the limited influence of possible errors in the removal of the topographic phase contribution, an estimate of the topography error is included in our processing algorithm to increase its robustness. Additionally, an atmospheric phase artifacts filtering operation is carried out on the computed space–time deformation measurements following the lines of the solution developed for the PS technique [16], [17]; in our case, the filtering operation takes benefit from the high spatial density of the imaged pixels.

We present results obtained on the data acquired from 1992 to 2000 by the ERS satellites and relative to the Campi Flegrei caldera and to the city of Naples, Italy that demonstrate the capability of the proposed approach to follow the dynamics of the detected deformations.

The paper is organized as follows. Section II explains the rationale of the technique that links the interferograms computed from separate data subsets. Section III describes the overall data processing procedure. Section IV is dedicated to the presentation of the obtained results. Conclusions and further developments are addressed in Section V.

II. Problem Formulation[1]

Let us start our analysis by considering $N+1$ SAR images relative to the same area and acquired at the ordered times $(t_0,\ldots,t_N)$. We also assume that each acquisition may interfere with at least another image; this implies that each SB subset is composed by a minimum of two acquisitions. Based on the above hypothesis, we conclude that the number of possible differential interferograms, say M, satisfies the following inequality (we have implicitly assumed N odd):

$$\frac{N+1}{2} \leq M \leq N\left(\frac{N+1}{2}\right). \tag{1}$$

Let us now briefly summarize the main characteristics of the DIFSAR interferograms considered and clarify the key issues of the investigated problem. Accordingly, we consider the generic j-interferogram computed, in the pixel of azimuth and range coordinates (x,r), from the SAR acquisitions at times t_B and t_A; this, following the topographic phase component removal [1], is given by

$$\begin{aligned}\delta\phi_j(x,r) &= \phi(t_B,x,r) - \phi(t_A,x,r) \\ &\approx \frac{4\pi}{\lambda}\left[d(t_B,x,r) - d(t_A,x,r)\right]\end{aligned} \tag{2}$$

wherein λ is the transmitted signal central wavelength, and $d(t_B,x,r)$ and $d(t_A,x,r)$ are the line-of-sight (LOS) cumulative deformations at times t_A and t_B with respect to the instant t_0, assumed as a reference. As a consequence, we have that $d(t_0,x,r)\equiv 0$, and therefore it is natural to identify $d(t_i,x,r)$, with $i=1,\ldots,N$, as the wanted deformation time series and to assume $\phi(t_i,x,r)$ as the associated phase component; thus $\phi(t_i,x,r)\approx 4\pi d(t_i,x,r)/\lambda$.

A few additional remarks on (2) are in order. First of all, we note that in the equation the decorrelation phenomena have been totally neglected as well as possible phase artifacts caused by changes in the atmosphere refraction index between the acquisitions and/or due to a nonprecise removal of the topographic phase component; these assumptions allow us to simplify the presented analysis without losing the rationale of the discussion and will be removed in Section III.

Moreover, we have also implicitly assumed that the phase signal is unwrapped and calibrated with respect to one pixel whose deformation is known (typically a high coherent pixel located in a nondeforming zone). A further feature of the proposed technique implies a pixel-by-pixel temporal analysis; accordingly, the dependence of (2) on the (x,r) variables is not explicitly mentioned hereafter. A discussion on the consequence of this pixel-by-pixel analysis is provided at the end of the section.

Let

$$\boldsymbol{\phi}^T = [\phi(t_1),\ldots,\phi(t_N)] \tag{3}$$

be the vector of the N unknown phase values associated with the deformation of the considered pixel and

$$\boldsymbol{\delta\phi}^T = [\delta\phi_1,\ldots,\delta\phi_M] \tag{4}$$

be the vector of the M (known) values of the computed DIFSAR interferograms. Equation (4) identifies the following two index vectors:

$$\mathrm{IS} = [\mathrm{IS}_1,\ldots,\mathrm{IS}_M] \quad \mathrm{IE} = [\mathrm{IE}_1,\ldots,\mathrm{IE}_M] \tag{5}$$

corresponding to the acquisition time-indexes associated with the image pairs used for the interferogram generation. Note also that we assume the master (IE) and slave (IS) images to be chronologically ordered, i.e., $\mathrm{IE}_j > \mathrm{IS}_j, \forall j = 1,\ldots,M$. In other words we have that

$$\delta\phi_j = \phi(t_{\mathrm{IE}_j}) - \phi(t_{\mathrm{IS}_j}), \qquad \forall j = 1,\ldots,M. \tag{6}$$

Accordingly, the expression (6) defines a system of M equations in N unknowns that may be organized in the following matrix representation [11]–[13]:

$$\mathbf{A}\boldsymbol{\phi} = \boldsymbol{\delta\phi} \tag{7}$$

$\mathbf{A}$ being an $M\times N$ matrix where $\forall j = 1,\ldots,M$ we have $A(j,\mathrm{IS}_j) = -1$ if $\mathrm{IS}_j \neq 0$, $A(j,\mathrm{IE}_j) = +1$ and zero otherwise. For instance, if $\delta\phi_1 = \phi_4 - \phi_2$ and $\delta\phi_2 = \phi_3 - \phi_0$, then $\mathbf{A}$ would have the following form:

$$\mathbf{A} = \begin{bmatrix} 0 & -1 & 0 & +1 & \ldots \\ 0 & 0 & +1 & 0 & \ldots \\ \ldots & \ldots & \ldots & \ldots & \ldots \\ \ldots & \ldots & \ldots & \ldots & \ldots \end{bmatrix}. \tag{8}$$

[1]The main contribution to the formulation of this section has been provided by G. Fornaro.

Expression (8) highlights that $\mathbf{A}$ is an incidence-like matrix, directly depending on the set of interferograms generated from the available data. Due to this characteristic, if all the acquisitions belong to a single SB subset, it turns out that $M \geq N$, and $\mathbf{A}$ is an N-rank matrix. Accordingly, the system of (7) is a well- ($M = N$) or an overdetermined ($M > N$) system, and its solution can be obtained, in general, in the LS sense as [19]

$$\hat{\boldsymbol{\phi}} = \mathbf{A}^{\#}\boldsymbol{\delta\phi} \text{ with } \mathbf{A}^{\#} = \left(\mathbf{A}^T\mathbf{A}\right)^{-1}\mathbf{A}^T. \tag{9}$$

Unfortunately, as pointed out in Section I, the availability of an entire dataset belonging to a single SB subset is typically uncommon; therefore, in order to increase the temporal sampling rate of the deformation signal, we must face the case of data belonging to different subsets. Clearly, we might still refer to the formulation in (7), but it is easily recognized that in this case $\mathbf{A}$ exhibits a rank deficiency, and therefore $\mathbf{A}^T\mathbf{A}$ is a singular matrix in (9). For instance, if we assume to face L different SB subsets, the rank of $\mathbf{A}$ will be $N - L + 1$, and the system will have infinite solutions (we assumed $N \leq M$; similar arguments apply to the other case).

A simple solution for inverting the system in (7) is provided by the SVD method [19], [20]. This allows us to evaluate the pseudoinverse of the matrix $\mathbf{A}$ that gives the minimum-norm LS solution of the system of (7).

In particular, by using the SVD decomposition, we decompose $\mathbf{A}$ as follows [20]:

$$\mathbf{A} = \mathbf{USV}^T \tag{10}$$

where $\mathbf{U}$ is an orthogonal $M \times M$ matrix whose first N columns, called the left-singular vectors of $\mathbf{A}$, are the eigenvectors of $\mathbf{AA}^T$; $\mathbf{V}$ is an orthogonal $N \times M$ matrix whose columns, the right-singular vectors of $\mathbf{A}$, are the eigenvectors of $\mathbf{A}^T\mathbf{A}$, and $\mathbf{S}$ is the $M \times M$ matrix whose entries (the singular values σ_i) are the square root of the corresponding eigenvalues of the $M \times M$ matrix $\mathbf{AA}^T$. Being generally $M > N$, $M - N$ eigenvalues are zero; moreover, due to the singular nature of $\mathbf{A}$, there are $L - 1$ additional null eigenvalues. In summary we have

$$\mathbf{S} = \operatorname{diag}\left(\sigma_1, \ldots, \sigma_{N-L+1}, 0, \ldots, 0\right). \tag{11}$$

The estimate $\boldsymbol{\phi}$ in the LS sense with minimum norm is finally obtained as follows:

$$\hat{\boldsymbol{\phi}} = \mathbf{A}^{+}\boldsymbol{\delta\phi} \text{ with } \mathbf{A}^{+} = \mathbf{VS}^{+}\mathbf{U}^T \tag{12}$$

where $\mathbf{S}^{+} = \operatorname{diag}(1/\sigma_1, \ldots, 1/\sigma_{N-L+1}, 0, \ldots, 0)$. Accordingly, we have [20]

$$\hat{\boldsymbol{\phi}} = \sum_{i=1}^{N-L+1} \frac{\boldsymbol{\delta\phi}^T\mathbf{u}_i}{\sigma_i}\mathbf{v}_i \tag{13}$$

where $\mathbf{u}_i$ and $\mathbf{v}_i$ are the column vectors of $\mathbf{U}$ and $\mathbf{V}$, respectively.

This solution is characterized by a minimum-norm constraint on the phase signal and, accordingly, on the detected deformation [see (2)]. As a consequence, the method forces the solution, in accordance with the starting equation system (7), to be as close to zero as possible. Unfortunately, this solution method may introduce large discontinuities in the cumulative deformations obtained, thus leading to a physically meaningless result; a pictorial example is shown in Fig. 1.

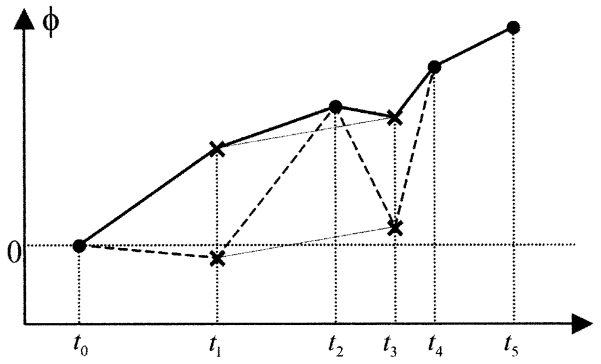

Fig. 1. Pictorial comparison between the minimum-norm phase (dashed line) and the minimum-norm velocity (continuous line) deformations. Two SB subsets, identified by dots and crosses, are considered in this example.

In order to guarantee a physically sound solution, we manipulate the equation system in (7) in such a way to replace the unknowns with the mean phase velocity between time-adjacent acquisitions. Accordingly, the new unknowns become

$$\underline{v}^T = \left[v_1 = \frac{\phi_1}{t_1 - t_0}, \ldots, v_N = \frac{\phi_N - \phi_{N-1}}{t_N - t_{N-1}}\right] \tag{14}$$

and in place of (6) we have

$$\sum_{k=\mathrm{IS}_j+1}^{\mathrm{IE}j} (t_k - t_{k-1})v_k = \delta\phi_j, \qquad \forall j = 1, \ldots, M \tag{15}$$

that, organized in a matrix form, finally leads to the expression

$$\mathbf{Bv} = \boldsymbol{\delta\phi}. \tag{16}$$

Note that the matrix $\mathbf{B}$ is again an $M \times N$ matrix; however, we have now that the generic (j, k) element will be $B(j, k) = t_{k+1} - t_k$ for $\mathrm{IS}_j + 1 \leq k \leq \mathrm{IE}_j, \forall j = 1, \ldots, M$, and $B(j, k) = 0$ elsewhere. Of course, in this case the SVD decomposition is applied to the matrix $\mathbf{B}$, and the minimum-norm constraint for the velocity vector $\mathbf{v}$ does not imply the presence of large discontinuities in the final solution (see the continuous line in Fig. 1); obviously, an additional integration step is necessary to achieve the final solution ϕ.

As an additional remark we note that we have considered a minimum-norm deformation velocity hypothesis for linking the different subsets information without using any further knowledge on the investigated deformation. It should be also pointed out that even the presence of a discrete deformation event concentrated in a few temporal points (i.e., an earthquake or a volcanic event) would be detected, provided that all the interferograms are properly unwrapped and calibrated with respect to one pixel whose deformation is known, as already stated.

Moreover, any available additional time-model information could be easily encompassed in the presented formulation. For instance, if the model parameter vector $\mathbf{p}$ exhibits a linear relationship with the velocity vector $\mathbf{v}$, i.e.,

$$\mathbf{v} = \mathbf{Mp} \tag{17}$$

where the columns of $\mathbf{M}$ describe the vector components of $\mathbf{v}$, then by substitution in (16) we have

$$\mathbf{BMp} = \boldsymbol{\delta\phi}. \tag{18}$$

Since the considered model is typically based on a few parameters (i.e., $\text{cardinality}\,[p] \leq N$), it generally leads to a simplification of the inversion of the system (18). In particular, for a smooth temporal model, the system (18) turns out to be generally nonsingular, thus allowing us to compute the solution via the left inverse matrix. For example, by assuming a cubic behavior for the time variation of the phase signal, for the generic j-component we have

$$\phi(t_i) = \bar{v}\cdot(t_i - t_0) + \frac{1}{2}\bar{a}\cdot(t_i - t_0)^2 + \frac{1}{6}\Delta\bar{a}\cdot(t_i - t_0)^3 \tag{19}$$

with $\bar{v}$, $\bar{a}$, and $\Delta\bar{a}$ being three unknown parameters accounting for the mean velocity, the mean acceleration, and mean acceleration variation, respectively. In this case, we have that the term $\mathbf{p}$ in (17) is trivially obtained from the expression

$$\mathbf{p}^T = [\bar{v}, \bar{a}, \Delta\bar{a}] \tag{20}$$

while $\mathbf{M}$ is

$$\mathbf{M} = \begin{bmatrix} 1 & \frac{t_1 - t_0}{2} & \frac{(t_1 - t_0)^2}{6} \\ 1 & \frac{t_2 + t_1 - 2t_0}{2} & \frac{(t_2 - t_0)^3 - (t_1 - t_0)^3}{6(t_2 - t_0)} \\ \cdots & \cdots & \cdots \\ 1 & \frac{t_N + t_{N-1} - 2t_0}{2} & \frac{(t_N - t_0)^3 - (t_{N-1} - t_0)^3}{6(t_N - t_{N-1})} \end{bmatrix}. \tag{21}$$

An easy extension of this model to pixel groups, or even to the whole available area, would allow us to benefit from the introduction of three-dimensional (3-D) space–time deformation models. As a matter of fact, to relate the information between two pixels, letting

$$\mathbf{B}_1\mathbf{v}_1 = \boldsymbol{\delta\phi}_1 \quad \mathbf{B}_2\mathbf{v}_2 = \boldsymbol{\delta\phi}_2 \quad \ldots \quad \mathbf{B}_K\mathbf{v}_K = \boldsymbol{\delta\phi}_K$$

be the K systems associated to the K pixels, we may reason on the following space–time extended problem:

$$\bar{\mathbf{B}}\bar{\mathbf{v}} = \boldsymbol{\delta\bar{\phi}} \tag{22}$$

with $\bar{\mathbf{B}} = \text{diag}\,[\mathbf{B}_1, \mathbf{B}_2, \ldots, \mathbf{B}_K]$, $\bar{\mathbf{v}}^T = \left[\mathbf{v}_1^T, \mathbf{v}_2^T, \ldots, \mathbf{v}_K^T\right]$, $\delta\bar{\phi}^T = \left[\delta\phi_1^T, \delta\phi_2^T, \ldots, \delta\phi_K^T\right]$. At this stage, following (17), the space–time deformation model is easily introduced as

$$\bar{\mathbf{v}} = \bar{\mathbf{M}}\bar{\mathbf{p}} \tag{23}$$

where $\bar{\mathbf{M}}$ and $\bar{\mathbf{p}}$ are the space–time model and parameter of the deformation. Along these lines, 3-D space–time phase-unwrapping algorithms could be also investigated.

III. Processing Algorithm

Before going into the details of the algorithm implementing the SVD-based approach discussed in Section II, it is important to reconsider, in a more realistic scenario, the DIFSAR phase expression in (2); accordingly, let us rewrite the interferometric signal as follows:

$$\begin{aligned} \delta\phi_j(x,r) &= \phi(t_B,x,r) - \phi(t_A,x,r) \\ &\approx \frac{4\pi}{\lambda}\left[d(t_B,x,r) - d(t_A,x,r)\right] + \frac{4\pi}{\lambda}\frac{B_{\perp j}\Delta z}{r\sin\vartheta} \\ &\quad + \left[\phi_{\text{atm}}(t_B,x,r) - \phi_{\text{atm}}(t_A,x,r)\right] \\ &\quad + \Delta n_j, \qquad \forall j = 1,\ldots,M \end{aligned} \tag{24}$$

wherein three additional phase components, with respect to (2), are present. The second one, i.e., the term $(4\pi/\lambda)(B_{\perp j}\Delta z/r\sin\vartheta)$, accounts for possible phase artifacts caused, within the DIFSAR phase generation process, by an error Δz in the knowledge of the scene topography; note that the impact of these artifacts depends on the orbit separation component $B_{\perp j}$ (usually referred to as perpendicular baseline or simply baseline) as well as on the sensor target distance r and on the look angle ϑ.

The third term in (24), represented by $[\phi_{\text{atm}}(t_B,x,r) - \phi_{\text{atm}}(t_A,x,r)]$, accounts for possible atmospheric inhomogeneities between the acquisitions at times t_A and t_B, and it is often referred to as atmospheric phase component.

Finally, the term Δn_j accounts for phase contributions caused by the baseline and temporal decorrelation phenomena and by the thermal noise effects.

In addition to the above considerations, in a real case, only the restriction to the $(-\pi,\pi)$ interval of the interferometric phase (wrapped phase) is directly measurable from the registered image pairs; therefore, since (16) relies on the availability of unwrapped signals, a retrieval operation must be carried out on the wrapped data. It is important to underline that the unwrapping operation is applied to each DIFSAR phase pattern but only involves those pixels that exhibit an estimated coherence value higher than an assumed threshold; this hypothesis allows us to exclude the pixels strongly affected by noise that, therefore, carry out no significant phase information and may have a negative impact on the performance of the unwrapping procedure. In particular, we have implemented the approach presented in [18] that is suitable for such a kind of sparsely coherent data. Pixels occurring in low coherence areas are just "filled in" via an interpolation step (implemented via a Delauny triangulation) starting from data located in high coherent unwrapped pixels. Note that our technique is independent of the phase-unwrapping algorithm used; accordingly, other choices could be possible.

The overall processing is implemented following the block diagram of Fig. 2. After the phase-unwrapping step, we jointly estimate a temporal low-pass (LP) component of the deformation signal and possible topographic artifacts via the least squares solution of the following system of equations derived from (18):

$$[\mathbf{BM}, \mathbf{c}]\,\mathbf{p}_c = \boldsymbol{\delta\phi} \tag{25}$$

wherein

$$\mathbf{c}^T = [(4\pi/\lambda)(B_{\perp 1}/r\sin\vartheta), \ldots, (4\pi/\lambda)(B_{\perp M}/r\sin\vartheta)]$$

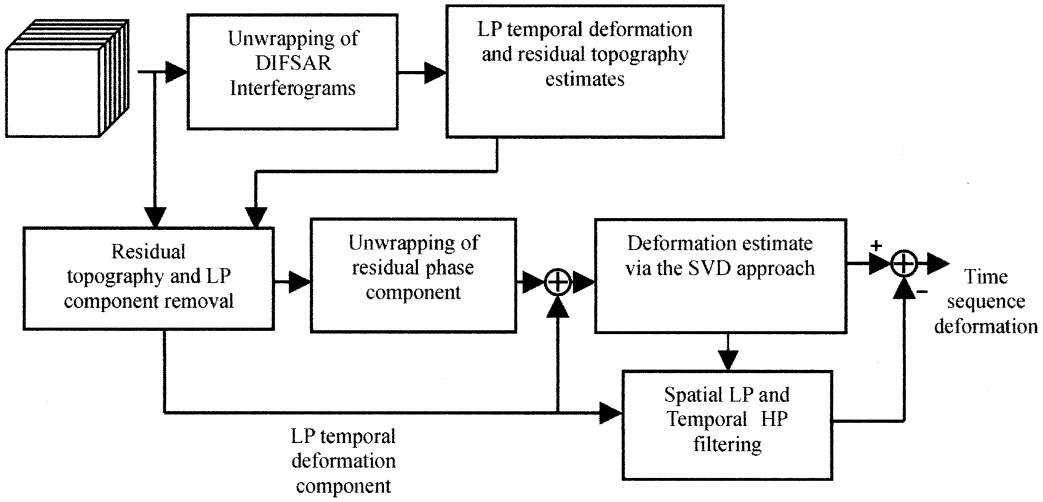

Fig. 2. Block diagram of the implemented algorithm.

and $\mathbf{p}_c^T = [\mathbf{p}^T, \Delta z]$, and wherein $\mathbf{p}$ and Δz are related to the LP component of the unwrapped signal (in reality, we typically consider, for sake of simplicity, its truncation to the first-order term) and to the topography artifacts, respectively. Even if the need for the estimation of the topographic factor Δz in (24) could appear irrelevant due the hypothesis of low baseline interferograms, we remark that the amplitude of local topographic artifacts may significantly exceed the expected digital elevation model (DEM) accuracy, thus causing a remarkable degradation of the produced DIFSAR fringes

Following this operation, the estimated LP phase patterns and topographic artifacts are subtracted modulo-2π from each input interferogram, thus typically leading to a fringe rate reduction. Accordingly, a new unwrapping step can be applied to the residual-wrapped phase patterns, the retrieval operation being significantly simplified (an effective phase noise filtering can be also easily performed at this stage due to the reduced fringe rate). By adding back the subtracted LP phase component, we finally achieve a refined unwrapped DIFSAR phase pattern.

At this stage, the SVD-based inversion discussed in the previous section can be finally applied. Accordingly, an estimate of the deformation velocity vector is achieved for each investigated pixel, and, following a trivial integration step, a measurement of the phase signal $\phi(t_i, x, r)$ is finally available $\forall t_i$ with $i = 1, \ldots, N$; see (24). However, in view of (24), it is evident that the results obtained do not only account for the wanted deformation signal $d(t_i, x, r)$ but also for the decorrelation effects and for possible atmospheric artifacts.

As far as the decorrelation phenomena are concerned, we remark that they are significantly mitigated by the complex multilook operation [21] carried out within the DIFSAR interferograms generation process and by the coherence-driven pixel selection. On the contrary, the presence of an atmospheric phase component represents a critical issue because it may significantly reduce the accuracy of the detected deformations and, in some case, completely mask them out (see [22]–[24]). Therefore, in order to mitigate the effect of these atmospheric artifacts, a filtering operation must be performed on the output of the SVD-based procedure. In this case, the applied filtering operation is derived from the PS approach discussed in [16] and [17], which is based on the observation that the atmospheric signal phase component is characterized by a high spatial correlation but exhibits a significantly low temporal correlation. Accordingly, the undesired atmospheric phase component is estimated as follows: first of all, we remove the LP component of the deformation signal already estimated via (25); following this step, the atmospheric phase component is detected as the result of the cascade of a lowpass filtering step, performed in the two-dimensional (2-D) spatial domain (i.e., azimuth and range), and a highpass filtering operation with respect to the time variable. Note that in our case the 2-D spatial filtering operation relies on the overall estimated phase signal and not only on a limited set of permanent scatters.

Once the atmospheric phase component has been evaluated, it is finally subtracted from the estimated phase signal; the conversion into a displacement signal is eventually achieved via the multiplication by the correction factor $\lambda/4\pi$; see (24).

IV. Results

The validation of this approach has been carried out by using an ERS-1/ERS-2 dataset composed by 44 acquisitions acquired, from June 8, 1992 until September 28, 2000, on a descending orbit (track 36 and frame 2781; see Table I) and distributed in three small baseline subsets; the 70 DIFSAR interferograms used in this study are characterized by a (perpendicular) baseline value smaller than 130 m. The test site, located in southern Italy, includes the active caldera of Campi Flegrei and the city of Naples (see Fig. 3). The overall analysis has been carried out on DIFSAR products obtained following a complex multilook operation with four looks in the range direction and 20 in the azimuth one; hence, the pixel dimension is about 85×80 m in azimuth and range directions, respectively; moreover, the coherence threshold has been fixed to 0.25. We remark that the pixel dimensions have been chosen rather large in order to map significantly wide areas without drastically expanding the overall amount of data; moreover, the large number of complex looks also allows us to reduce the phase noise.

TABLE I
ERS-1/ERS-2 DATA USED. THE DIFFERENT SB SUBSETS ARE HIGHLIGHTED

Mission	Orbit	Day	Month	Year	$B_\perp$	SB Subset
ERS1	4690	8	6	1992	0	1
ERS1	6694	26	10	1992	-124	1
ERS1	7195	30	11	1992	159	1
ERS1	8197	8	2	1993	-544	2
ERS1	8698	15	3	1993	-119	1
ERS1	9700	24	5	1993	-518	2
ERS1	10201	28	6	1993	-591	2
ERS1	10702	2	8	1993	-118	1
ERS1	11203	6	9	1993	31	1
ERS1	12205	15	11	1993	-58	1
ERS1	19563	12	4	1995	-525	2
ERS1	21066	26	7	1995	-149	1
ERS2	1393	27	7	1995	-185	1
ERS2	1894	31	8	1995	-555	2
ERS2	2395	5	10	1995	473	1
ERS2	3397	14	12	1995	19	1
ERS1	24072	21	2	1996	420	1
ERS1	25074	1	5	1996	400	1
ERS2	5401	2	5	1996	310	1
ERS2	6904	15	8	1996	-546	2
ERS2	7906	24	10	1996	371	1
ERS2	8908	2	1	1997	-387	2
ERS2	9409	6	2	1997	-99	1
ERS2	10411	17	4	1997	215	1
ERS2	10912	22	5	1997	-429	2
ERS2	11914	31	7	1997	-392	2
ERS2	13417	13	11	1997	-529	2
ERS2	13918	18	12	1997	-471	2
ERS2	15922	7	5	1998	153	1
ERS2	16924	16	7	1998	-1064	3
ERS2	17926	24	9	1998	-69	1
ERS2	18928	3	12	1998	-642	2
ERS2	20431	18	3	1999	-250	1
ERS2	21934	1	7	1999	-177	1
ERS2	22435	5	8	1999	-191	1
ERS2	22936	9	9	1999	-972	3
ERS2	23437	14	10	1999	-617	2
ERS2	24439	23	12	1999	-474	2
ERS2	24940	27	1	2000	-430	2
ERS2	25441	2	3	2000	-986	3
ERS2	26944	15	6	2000	-497	2
ERS2	27445	20	7	2000	-929	3
ERS2	27946	24	8	2000	164	1
ERS2	28447	28	9	2000	-257	1

In the results presented, the topographic phase component has been removed by using a DEM provided by the Italian Army, whose nominal height accuracy is of about 10–20 m, and the ERS-1/ERS-2 precise orbit state vectors computed by the Technical University of Delft. In this case, despite the expected accuracy, significant topography artifacts have been detected (see Fig. 4), thus making the refined topography phase removal operation a relevant step. Note also that the approach is applied to pixels exhibiting an estimated coherence value higher than the selected threshold in at least 30% of the computed interferograms. This assumption is consistent with the chosen strategy of maximizing the spatial information.

In order to provide an overall picture of the detected deformation, we present in Fig. 5 the false-color map representing the root-mean-square (rms) value of the computed deformation, for

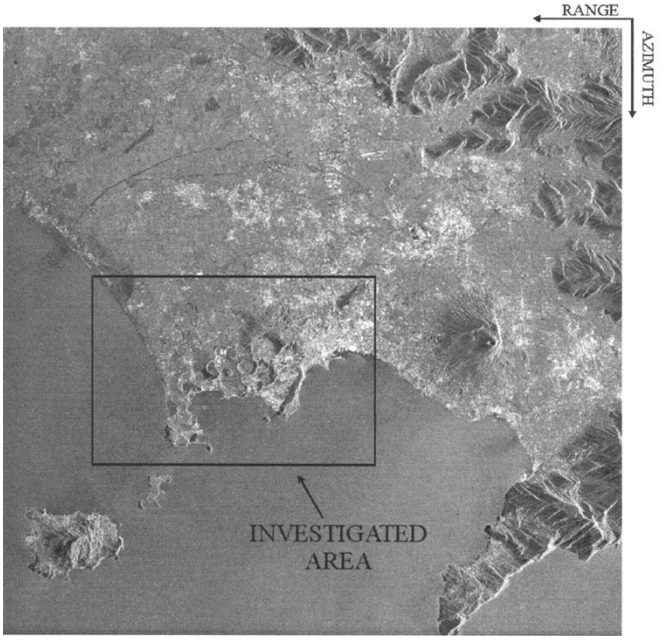

Fig. 3. SAR image of the overall zone. The investigated area is highlighted.

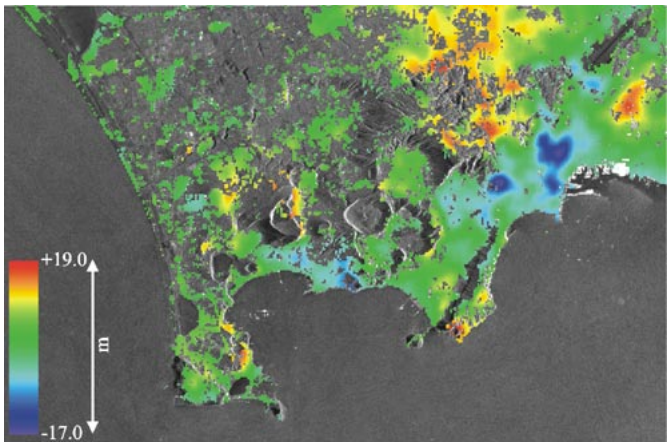

Fig. 4. False-color map of the detected topography errors superimposed on the SAR image amplitude of the investigated area.

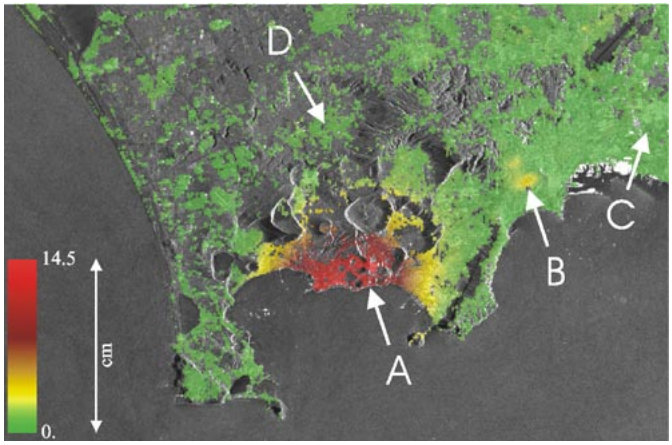

Fig. 5. False-color map of the measured deformation rms superimposed on the SAR image amplitude of the investigated area. The temporal evolution of the deformations in the selected points identified by A, B, and C are shown in Figs. 6(a)–(c), respectively. In points A and D, GPS measurements carried out in March and September 2000 were available to us [25].

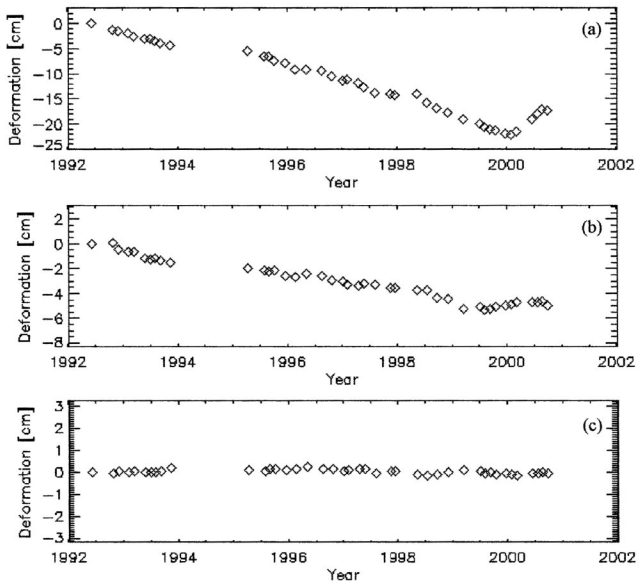

Fig. 6. Time-series deformation measured in (a) point A, (b) point B, and (c) point C of Fig. 5.

each investigated pixel, superimposed on the grayscale representation of the SAR image amplitude. Note that this rms representation is visually effective and allows us to provide, for each pixel of the investigated area, an integral information (with respect to time) of the detected deformation whose amount becomes more significant as we move from green areas (stable zones) to red ones (highly deforming zones); obviously, areas where the measurement accuracy is affected by decorrelation noise have been excluded from the false-color map.

Fig. 5 clearly shows that a significant deformation pattern is present in two areas that can be easily identified: the largest one, on the left-hand side, represents the Campi Flegrei caldera, while the one on the right side, significantly smaller, is located in the Vomero zone, a densely populated quarter within the city of Naples. In order to demonstrate the capability of the proposed approach to follow the temporal evolution of the detected deformation, some examples are provided in the following. Fig. 6 presents the chronological sequence of the computed deformations for a point (marked by A in Fig. 5) located in the area of maximum subsidence/uplift of the Campi Flegrei caldera. Note that the observed deformations are characterized by a rather continuous subsidence phenomenon from 1992 until the beginning of 2000, when a change of the deformation trend occurs resulting in an uplift phase. These results are confirmed by geodetic measurements carried out by the researchers of the Osservatorio Vesuviano (OV), which is the institution in charge of monitoring the deformations occurring in the area. In this case, due to the availability of differential global positioning system (GPS) measurements performed during the uplift crisis of the year 2000 (these data have a height accuracy of about 1 cm [25]), it was possible to perform a comparison between the SAR results and the geodetic measurements carried out in March and September 2000 in the points A and D of Fig. 5, the latter being located outside the highly deforming zone. The results obtained by projecting, in the radar line of site, the GPS deformations of A (relative to D) give 4.14 cm of displacement whereas the corresponding SAR measurements result in 4.05 cm; the good agreement between the two different types of data is evident.

Let us now consider the deformations occurring in the Vomero area; in this case, the presence of a deformation effect was originally revealed by SAR techniques [10], but again our technique allows us not only to identify this deformation but also to track its temporal evolution; this is evident when we consider Fig. 6(b), wherein the evolution of the deformation for a point (marked by B in Fig. 5) located in the area of maximum deformation of this zone is presented. Note that in this case no geodetic measurements are available, and therefore no comparison was possible.

Finally, we have considered a point in the downtown area of the city (marked by C in Fig. 5) that is supposed to be significantly stable. This hypothesis is fully confirmed by our observations clearly showing [see Fig. 6(c)] that no deformation can be detected in this zone during the investigated time interval.

As a final remark, we note that the presented technique has been also recently applied to study the deformations occurring at the Vesuvius volcano [26].

V. Conclusion and Future Developments

This paper describes an innovative technique for investigating surface deformations via the differential interferometric SAR technique. This approach is based on the use of a large number of SAR acquisitions distributed in small baseline subsets; it allows the easy combination of DIFSAR interferograms computed via standard processing techniques and computation of a time sequence of deformation.

Key features of the proposed technique are the large number of useful SAR data acquisitions that allows an increase of the temporal sampling rate of the monitoring, and the high degree of spatial coverage over the area of interest, related to the use of small baseline interferograms only.

The technique we present is applied pixel by pixel to all the areas exhibiting a sufficiently high coherence degree and is robust with respect to possible errors of the DEM used in the derivation of the differential interferograms. Moreover, the availability of both time and space information allows us to effectively remove the atmospheric artifacts in the results via a proper space–time filtering operation. More sophisticated, or even optimal, atmospheric filtering techniques could be included in the processing algorithm and can be the object of further developments.

Since it is based on a simple inversion of a linear model, it is intrinsically plausible to introduce an *a priori* knowledge about the temporal behavior of the deformation into the technique, as pointed out in Section II. Moreover, an easy extension of this model to pixel groups, or even to the whole available areas, allows us to benefit from the introduction of 3-D space–time deformation models.

As a final remark, we underline that the proposed technique is not suitable, at the present stage, for detecting local deformations on a small spatial scale as, for example, in the case of small buildings suffering a structural stress; however, the extension of

our approach to the detection and monitoring of such local deformation seems rather simple, and preliminary results on these issues look very promising [27].

ACKNOWLEDGMENT

The DEM of the area has been provided by the I.G.M. of the Italian Army and the precise ERS-1/ERS-2 satellite orbit state vectors by the Technical University of Delft, The Netherlands. The authors thank S. Usai and F. Soldovieri for interesting discussions, J. Bequignon for his support, and P. De Martino, G. P. Ricciardi, and S. Borgström for providing them with GPS measurements of the Campi Flegrei area. They also thank the anonymous reviewer that carefully proofread the manuscript.

REFERENCES

[1] A. K. Gabriel, R. M. Goldstein, and H. A. Zebker, "Mapping small elevation changes over large areas: Differential interferometry," *J. Geophys. Res.*, vol. 94, pp. 9183–9191, July 1989.

[2] D. Massonnet, M. Rossi, C. Carmona, F. Ardagna, G. Peltzer, K. Feigl, and T. Rabaute, "The displacement field of the landers earthquake mapped by radar interferometry," *Nature*, vol. 364, pp. 138–142, July 1993.

[3] D. Massonnet, P. Briole, and A. Arnaud, "Deflation of Mount Etna monitored by spaceborne radar interferometry," *Nature*, vol. 375, pp. 567–570, June 1995.

[4] G. Peltzer and P. A. Rosen, "Surface displacement of the 17 Eureka valley, California, earthquake observed by SAR interferometry," *Science*, vol. 268, pp. 1333–1336, June 1995.

[5] E. Rignot, "Fast recession of a west Antarctic glacier," *Science*, vol. 281, pp. 549–551, July 1998.

[6] S. Stramondo, M. Tesauro, P. Briole, E. Sansosti, S. Salvi, R. Lanari, M. Anzidei, P. Baldi, G. Fornaro, A. Avallone, M. F. Buongiorno, G. Franceschetti, and E. Boschi, "The September 26, 1997 Colfiorito, Italy, earthquakes: Modeled coseismic surface displacement from SAR interferometry and GPS," *Geophys. Res. Lett.*, vol. 26, pp. 883–886, Apr. 1999.

[7] A. Borgia, R. Lanari, E. Sansosti, M. Tesauro, P. Berardino, G. Fornaro, M. Neri, and J. Murray, "Actively growing anticlines beneath Catania from the distal motion of Mount Etna's decollement measured by SAR interferometry and GPS," *Geophys. Res. Lett.*, vol. 27, pp. 3409–3412, Oct. 2000.

[8] H. Vadon and F. Sigmundsson, "Crustal deformation from 1992 to 1995 at the Midatlantic ridge, southwest Iceland, mapped by satellite radar interferometry," *Science*, vol. 275, pp. 193–197, Jan. 1997.

[9] R. Lanari, P. Lundgren, and E. Sansosti, "Dynamic deformation of Etna volcano observed by satellite radar interferometry," *Geophys. Res. Lett.*, vol. 25, pp. 1541–1544, May 1998.

[10] M. Tesauro, P. Berardino, R. Lanari, E. Sansosti, G. Fornaro, and G. Franceschetti, "Urban subsidence inside the city of Napoli (Italy) observed by satellite radar interferometry," *Geophys. Res. Lett*, vol. 27, pp. 1961–1964, July 2000.

[11] P. Lundgren, S. Usai, E. Sansosti, R. Lanari, M. Tesauro, G. Fornaro, and P. Berardino, "Modeling surface deformation observed with SAR interferometry at Campi Flegrei Caldera," *J. Geophys. Res.*, vol. 106, pp. 19 355–19 367, Sept. 2001.

[12] S. Usai, "A new approach for long term monitoring of deformations by differential SAR interferometry," Ph.D. thesis, Delft Univ. Press, Delft, The Netherlands, 2001.

[13] P. Berardino, G. Fornaro, A. Fusco, D. Galluzzo, R. Lanari, E. Sansosti, and S. Usai, "A new approach for analyzing the temporal evolution of earth surface deformations based on the combination of DIFSAR interferograms," in *Proc. IGARSS*, Sidney, Australia, July 2001, pp. 2551–2553.

[14] S. Usai and R. Klees, "SAR interferometry on a very long time scale: A Study of the interferometric characteristics of man-made features," *IEEE Trans. Geosci. Remote Sensing*, vol. 37, pp. 2118–2123, July 1999.

[15] S. Usai, "An analysis of the interferometric characteristics of anthropogenic features," *IEEE Trans. Geosci. Remote Sensing*, vol. 38, pp. 1491–1497, May 2000.

[16] A. Ferretti, C. Prati, and F. Rocca, "Permanent scatterers in SAR interferometry," *IEEE Trans. Geosci. Remote Sensing*, vol. 39, pp. 8–20, Jan. 2001.

[17] ——, "Nonlinear subsidence rate estimation using permanent scatterers in differential SAR interferometry," *IEEE Trans. Geosci. Remote Sensing*, vol. 38, pp. 2202–2212, Sept. 2000.

[18] M. Costantini and P. A. Rosen, "A generalized phase unwrapping approach for sparse data," in *Proc. IGARSS*, Hamburg, Germany, June 1999, pp. 267–269.

[19] G. Strang, *Linear Algebra and Its Appications*. Orlando, FL: Harcourt Brace Jovanovich, 1988.

[20] G. H. Golub and C. F. Van Loan, *Matrix Computation*. Baltimore, MD: Johns Hopkins Univ. Press, 1996, ch. 2.

[21] G. Franceschetti and G. Fornaro, "Synthetic aperture radar interferometry," in *Synthetic Aperture Radar Processing*, G. Franceschetti and R. Lanari, Eds. Boca Raton, FL: CRC, 1999, ch. 4.

[22] R. M. Goldstein, "Atmospheric limitations to repeat-track radar interferometry," *Geophys. Res. Lett.*, vol. 22, pp. 2517–2520, Sept. 1995.

[23] H. Tarayare and D. Massonnet, "Atmospheric propagation heterogeneities revealed by ERS-1 interferometry," *Geophys. Res. Lett*, vol. 23, pp. 989–992, May 1996.

[24] H. A. Zebker, P. A. Rosen, and S. Hensley, "Atmospheric effects in interferometric synthetic aperture radar surface deformation and topographic maps," *J. Geophys. Res*, vol. 102, pp. 7547–7563, Apr. 1997.

[25] Osservatorio Vesuviano, Crisi bradisismica della Caldera dei Campi Flegrei 2000, July 2000.

[26] R. Lanari, G. De Natale, P. Berardino, E. Sansosti, G. P. Ricciardi, S. Borgstrom, P. Capuano, F. Pingue, and C. Troise, "Evidence for a peculiar style of ground deformation inferred at Vesuvius volcano," *Geophys. Res. Lett*, vol. 29, no. 9, 2002.

[27] Mora, O. R. Lanari, J. J. Mallorquí, P. Berardino, and E. Sansosti, "A new algorithm for monitoring localized deformation phenomena based on small baseline differential SAR interferograms," in *Proc. IGARSS*, Toronto, ON, Canada, July 2002, pp. 1237–1239.

Paolo Berardino (S'96–A'01–M'02) was born in Avellino, Italy, in 1971. He received the Laurea degree in nautical sciences from the Naval University of Napoli, Naples, Italy, in 1998, with a thesis on synthetic aperture radar geocoding.

Since 1999, he has been with Istituto per il Rilevamento Elettromagnetico dell'Ambiente (IREA, formerly IRECE), an Institute of the Italian National Research Council (CNR), Naples, Italy. His studies regard geocoding of SAR images and surface deformation observed by SAR interferometry (IFSAR). In particular, he applied the IFSAR technique in volcanic areas such as Mount Etna and Campi Flegrei for monitoring and modeling the deformation sources activity, and in the urban area of Naples to study the subsidence effects related to the underground excavations. He is currently working on a new approach for analyzing the temporal evolution of earth surface deformations based on the combination of DIFSAR interferograms.

Gianfranco Fornaro received the Laurea degree in electronic engineering from the University of Napoli, Naples, Italy, in 1992, and the Ph.D. degree from the University of Rome "La Sapienza," Rome, Italy, in 1997.

He is currently a Senior Researcher at the Istituto per il Rilevamento Elettromagnetico dell'Ambiente (IREA, formerly IRECE), an Institute of the Italian National Research Council (CNR), Naples, Italy, and an Adjunct Professor of communications at the University of Cassino, Cassino, Italy. His main research interests are in the signal processing field with applications to synthetic aperture radar (SAR) data processing, SAR interferometry, and differential SAR interferometry. He was a Visiting Scientist at the German Aerospace Center (DLR), Oberpfaffenhofen, Germany, and at the Politecnico of Milano, Milan, Italy, and has been lecturer at the Istituto Tecnologico de Aeronautica (ITA), São José dos Campos, São Paulo, Brazil.

Dr. Fornaro was awarded the Mountbatten Premium by the Institution of Electrical Engineers (IEE) in 1997.

Riccardo Lanari (M'91–SM'01) graduated in 1989 (summa cum laude) in electronic engineering at the University of Napoli "Federico II," Naples, Italy.

He joined the Istituto per il Rilevamento Elettromagnetico dell'Ambiente (IREA, formerly IRECE), an Institute of the Italian National Research Council (CNR), Naples, Italy, in 1989, where he is a Senior Researcher and is a member of the institute committee. He is also an Adjunct Professor of electrical communications at the Università degli Studi del Sannio, Benevento, Italy and Lecturer of the SAR module course of the International Master in Airbone Photogrammetry and Remote Sensing, offered by the Institute of Geomatics, Barcelona, Spain. His main research activities are in the synthetic aperture radar (SAR) data processing field as well as in SAR interferometry techniques; on this topic he has authored 30 international journal papers and, more recently, a book entitled *Synthetic Aperture Radar Processing*. He was Visiting Scientist at different foreign research institutes: Institute of Space and Astronautical Science, Kanagawa, Japan (1993), German Aerospace Center (DLR), Oberpfaffenhofen, Germany (1991 and 1994), and the Jet Propulsion Laboratory, Pasadena, CA (1997), where he also received a National Aeronautics and Space Administration recognition for the development of the ScanSAR processor used in the Shuttle Radar Topography Mission. He holds two patents on SAR data processing techniques.

Dr. Lanari has been invited as chairman and co-chairman at several international conferences.

Eugenio Sansosti (M'98–SM'02) received the "Laurea" degree (summa cum laude) in electronic engineering from the University of Napoli "Federico II," Naples, Italy, in 1995.

Since 1997, he has been with Istituto per il Rilevamento Elettromagnetico dell'Ambiente (IREA, formerly IRECE), an Institute of the Italian National Research Council (CNR), Naples, Italy, where he currently holds a Full Researcher position. He is also an Adjunct Professor of Communications at University of Cassino, Cassino, Italy.

He was Guest Scientist at the Jet Propulsion Laboratory, Pasadena, CA from August 1997 to February 1998, and again in February 2000 in support of the National Aeronautics and Space Administration Shuttle Radar Topography Mission. In November and December 2000, he worked as an Image Processing Adviser at Istituto Tecnologico de Aeronautica (ITA), São José dos Campos, São Paulo, Brazil. His main research interests are in airborne and spaceborne synthetic aperture radar (SAR) data processing, SAR interferometry, and differential SAR interferometry.